Energy Reports 8 (2022) 14259–14273

Contents lists available at ScienceDirect

Energy Reports

journal homepage: www.elsevier.com/locate/egyr

# Reversible solid oxide cell coupled to an offshore wind turbine as a poly-generation energy system for auxiliary backup generation and hydrogen production

Mario Lamagna [a,*], Andrea Monforti Ferrario [b,c], Davide Astiaso Garcia [d], Stephen Mcphail [e], Gabriele Comodi [b]

[a] Department of Astronautical, Electrical and Energy Engineering (DIAEE), Sapienza University of Rome, Via Eudossiana, 18 – 00184 Rome, Italy
[b] Department of Industrial Engineering and Mathematical Sciences (DIISM), Università Politecnica delle Marche, Via Brecce Bianche 12 - 60131 Ancona, Italy
[c] ENEA, Laboratory of Energy Storage, Batteries and Hydrogen Production & Use, Department of Energy Technologies and Renewable Sources (TERIN-PSU-ABI), Italian National Agency for New Technologies, Energy and Sustainable Economic Development, C.R. Casaccia, Via Anguillarese 301 – 00123 Rome, Italy
[d] Department of Planning, Design, Technology of Architecture (DPDTA), Sapienza University of Rome, Via Flaminia 72 – 00196 Rome, Italy
[e] ENEA, Laboratory of Energy Storage, Batteries and Hydrogen Production & Use, Department of Energy Technologies and Renewable Sources (TERIN-PSU-ABI), C.R. Casaccia, Via Anguillarese 301 – 00123 Rome, Italy

ARTICLE INFO

*Article history:*
Received 1 March 2022
Received in revised form 21 August 2022
Accepted 18 October 2022
Available online xxxx

*Keywords:*
rSOC
Offshore wind power
PtP
PtG
Auxiliary system supply
Hydrogen

ABSTRACT

The coupling of a reversible Solid Oxide Cell (rSOC) with an offshore wind turbine is investigated to evaluate the mutual benefits in terms of local energy management. This integrated system has been simulated with a dynamic model under a control algorithm which manages the rSOC operation in relation to the wind resource, implementing a local hydrogen storage with a double function: (i) assure power supply to the wind turbine auxiliary systems during power shortages, (ii) valorize the heat produced to cover the desalinization system needs. With an export-based strategy, which maximize the rSOC capacity factor, up to 15 tons of hydrogen could be produced for other purposes. The results show the compatibility between the auxiliary systems supply of a 2.3 MW wind turbine and a 120/21 kWe rSOC system which can cover the auxiliaries demand during wind shortages or maintenance. The total volume required by such a system occupy less than the 2%, if compared with the turbine tower volume. Additionally, thermal availability exceeds the desalination needs, representing a promising solution for small-scale onsite desalination in offshore environments.



## 1. Introduction

Wind Turbine (WT) technology and in particular Offshore Wind Turbine (OWT) technology is today a consolidated renewable energy technology which is rapidly gaining momentum going from 1% of global wind installations by capacity in 2009, to over 10% in 2019 (GWEC, 2021). This is also due to the optimal wind resource availability at sea (IEA, 2020), which allows the installation of larger size wind turbines. On average, turbine capacity has increased by 16% every year since 2014 until reaching a rated capacity of 7.8 MW in 2019, 1 MW larger than the value recorded in 2018 (Wind europe, 2021).

Nevertheless, their installation and operation provide different technical challenges including the maintenance (Ren et al., 2021), also considering the fact that they are often installed in remote areas located up to 60 km from the nearest shore to exploit the best wind availability (Barbarelli and Nastasi, 2021). The main problems can occur when the wind farm, totally or partially, is not producing energy (Dedecca et al., 2017), this could happen when the wind speed is above or below the producibility curve or during disconnection procedures such as switching actions, protective switching of a circuit breaker in the grid or protective switching of a circuit breaker because of an internal wind turbine failure (Bodewes, 2017). In this situation the turbine will be in standby, but nonetheless the auxiliary systems must be continuously supplied to maintain operative the unstoppable loads such us the monitoring and communication instrumentations or the safety devices. Although both the rated power and total energy demand volume related to the auxiliaries is low with respect to the OWT power and energy production volume, their supply during the aforementioned conditions can pose a critical situation. Usually, an Uninterruptible Power Supply (UPS) is installed to manage those kinds of problems, typically based on batteries

* Corresponding author.
*E-mail address:* mario.lamagna@uniroma1.it (M. Lamagna).

https://doi.org/10.1016/j.egyr.2022.10.355

## Nomenclature

### Acronyms

| | |
|---|---|
| P | power (kW) |
| $v$ | wind speed (m/s) |

### Abbreviations

| | |
|---|---|
| AEP | annual energy production |
| ALK | alkaline |
| CAPEX | capital expenditure |
| DES | direct Electrolysis of Seawater |
| EMS | energy management system |
| $GH_2$ | green hydrogen |
| $CGH_2$ | compressed green hydrogen |
| KPI | key performance indicator |
| Li-Ion | lithium battery |
| LCOH | levelized cost of hydrogen |
| LCOS | levelized cost of storage |
| MED | multistage effect |
| MSF | multistage flash |
| O&M | operation and maintenance |
| OPEX | operational expenditure |
| OR | reverse osmosis |
| OWT | offshore wind turbine |
| PEM | proton Exchange Membrane |
| PMT | periodic payment for an annuity |
| PV | photovoltaic panels |
| $QH_{2PMax}$ | maximum hydrogen production flow |
| rSOC | reversible solid oxide fuel cell |
| SEC | specific energy consumption |
| SOC | state of charge |
| SOEC | solid oxide electrolyzer |
| SOFC | solid oxide fuel cell |
| $UF_f$ | fuel utilization factor |
| $UF_s$ | steam utilization factor |
| UPS | uninterruptible power system |
| WRR | water recovery rate |

### Symbols

| | |
|---|---|
| $\beta$ | pressure ratio |

### Subscripts and superscript

| | |
|---|---|
| $_{ci}$ | cut-in |
| $_{co}$ | cut-out |
| $_{np}$ | nominal power |
| $_{wt}$ | wind turbine |

(Xu et al., 2020) and diesel generators (Shezan, 2021). Despite being cheap and reliable, diesel generators need maintenance and refuelling which can become an issue in offshore conditions. Likewise, batteries are sensitive to temperature changes (Ma et al., 2018) with limited energy density (Rezk et al., 2021), thus many packages could be required, and over time their capacity may degrade (Chen et al., 2021). From the above considerations it follows that for a wind turbine to be safely operated when power outage occurs a reliable UPS, able to deliver power for a long time, is required (Zhao et al., 2022). Otherwise, a bidirectional grid connection cable (with all related bidirectional power electronic conversion systems) is required, to supply the auxiliaries during OWT idle conditions, which sensibly increases the electrical balance of plant costs. It must be considered that these issues, with the increasing of the sizes and distances from the shore they can worsen, increasing the significance to find a valuable UPS solution. Similar constraints are shared with other isolated realities, such as island (Groppi et al., 2021) or remote areas (Rezk, 2019) energy systems. Additionally, those situations are accentuated by variable loads and greater sizes, which make even more relevant the adoption of energy storages (Manfren et al., 2021) and short-term forecasting due to the total system inertia (Heydari et al., 2020).

Similarly to the offshore wind turbines, hydrogen is being proposed with a lead role in the energy transition (Hydrogen Council, 2021). When produced by the coupling of renewable energy sources and water electrolysis (Nastasi, 2019), green hydrogen ($GH_2$) can become a valid ally in terms of renewable energy storage and management (Kakoulaki et al., 2021).

To date, different investigations have been done to understand the possible coupling between renewable and hydrogen application (Nastasi, 2015) and recently also between OWT and hydrogen technologies (Wu et al., 2022). In the study presented by (d'Amore Domenech et al., 2020) the objective was to evaluate the different electrolysis technologies available on the market (i) the alkaline electrolysis (ALK) (ii) the Proton Exchange Membrane (PEM) electrolysis, the (iii) Solid Oxide (SOEC) electrolysis and the (iv) Direct Electrolysis of Seawater (DES), to be installed coupled to an offshore wind turbine for $GH_2$ production.

Likewise, in Meier (2014) and Dinh et al. (2020) the $GH_2$ production is analysed considering the Norwegian and Irish offshore framework respectively, considering also different transport options for the yield of the produced hydrogen by means of ships or pipeline toward the shore. Similarly, a study was conducted in Denmark (Hou et al., 2017) to assess the optimum size and financial support in order to sustain a system composed of an offshore wind farm, an electrolyzer and a fuel cell to convert the hydrogen back into electricity. While Baptista et al. (2021) and Crivellari and Cozzani (2020) the attention was focused mainly on the different possible pathways for the hydrogen produced offshore to be transported towards the coast.

Although there are some studies which cover the coupling of SOEC systems with MW-scale wind turbines (Shepherd et al., 2021; Xueqing et al., 2021), the main novelty of this work consists in assessing the use of a reversible Solid Oxide Cell (rSOC) system for direct use of the produced hydrogen locally at turbine level to produce electricity to supply the auxiliaries when needed. A rSOC was selected for this study to avoid installing two different components, i.e. the fuel cell and the electrolyzer (Zahedi et al., 2021; Hou et al., 2017).

Although less mature than alkaline and PEM fuel cell/electrolysis technology, rSOC can already offer higher efficiency and exploitable heat (Timothy et al., 2021).

As matter of fact, considering the rSOC high operating temperature (Rispoli et al., 2020), it is possible to valorize the available high-grade heat for seawater desalination. All the above-mentioned studies did not address the water treatment topic, which is required to produce hydrogen in the electrolysis system (Farhat et al., 2021), underlining another difference from this work to the previous ones. The water treatment coupled with the rSOC heat production has already started to draw the attention of many works, as reported in (Beyrami et al., 2019). More specifically, in (Ullvius and Rokni, 2019) the coupling of an rSOC with solar thermal systems and a desalination unit is examined, while in (Chitgar and Moghimi, 2020) the thermal renewable contribution is substituted by a gas turbine exhaust gases. With an alternative approach in (Campione et al., 2020),

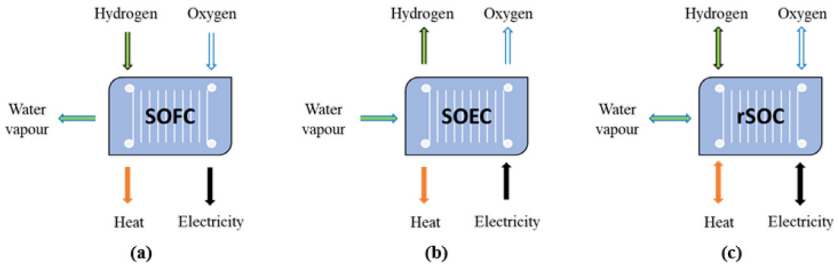


**Fig. 1.** Schematic representation of (a) SOFC system; (b) SOEC system; (c) rSOC system.

the rSOC operation in a microgrid, coupled with PV panels, and directly supplied with seawater, is simulated. Nevertheless, the desalination process was not considered locally at offshore level in none of the analysed works.

Differently in this paper, an integrated system assessment made of an OWT, rSOC, hydrogen storage, and a desalination unit will be developed. The integrated system has been simulated with a dynamic model under a rule-based control algorithm which manages the rSOC operation in relation to the wind resource with a double function: (i) assure power supply to the wind turbine auxiliary systems during power shortages, (ii) valorize the heat produced to cover the desalinization system needs. Finally, insights from an economic point of view are given.

### 1.1. Brief technology overview — reversible Solid Oxide Cell (rSOC)

The rSOC is an electrochemical conversion system based on the Solid Oxide Cell technology which can be operated reversibly both in fuel cell (SOFC) and electrolyser (SOEC) mode. Its electrodes can be effectively operated in both operating modes, thanks to the compatibility of electrocatalysts for both electrochemical conversion direction (Wang et al., 2017). In addition, the high operating temperatures (around 800 °C) favours the reaction kinetics – leading to low overpotential losses – and ensures that all reactants are always in gaseous phase, especially water which is produced/consumed in the form of steam (Yue et al., 2021).

Thus, by implementing a suitable balance of plant the system can be unitized in a single poly-generation system which can act as a flexible energy storage system switching between SOEC mode, hence generating hydrogen while consuming steam and electricity, and SOFC mode, hence generating electricity and steam while consuming hydrogen. In both operating modes, a high-grade heat recovery is possible thanks to the high operating temperatures of the process (Wang et al., 2020). While the SOFC mode is always exothermal, the SOEC mode can be either endothermal, thermoneutral or exothermal according to the operating voltage point. However, SOEC mode is typically maintained in thermoneutral regime or in slightly exothermal regime to obtain heat also in this mode, avoiding further complications of the overall system thermal management (Pourrahmani et al., 2021). Also oxygen is a produced/consumed gas (Fan et al., 2021) that can be exploited if needed. In Fig. 1 the different rSOC operation modes system are illustrated.

The rSOC – seen as an integrated storage system – is one of the most promising solutions among the reversible hydrogen technologies in terms of (i) durability, (ii) capital cost and, (iii) roundtrip conversion efficiency and (iv) power density (Peterson, 2020; Venkataraman et al., 2019). The rSOC technology is also appreciated for its scalability, offering a wide capacity range from few kW to MW-scales (Wang et al., 2019). This is possible thanks to the modularity of its electrochemical technology, representing a highly versatile option to cover different types of applications.

As previously discussed, a rSOC system could find several synergies with the analysed case. Its power-intensity and high

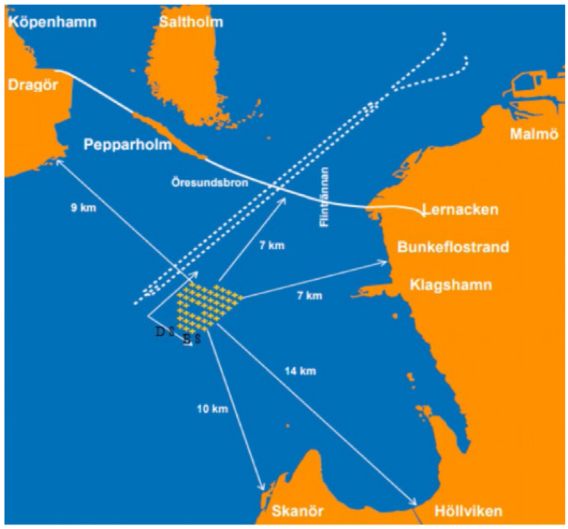


**Fig. 2.** Lillgrund OW farm (image from Jesson et al. (2008)).

electrical efficiency are well matched with the growing electricity demand for OWT auxiliary systems, given the increasing trend of the nominal power recorded. In addition, the high-grade heat related to the process temperatures (Mogensen et al., 2019) can be used to cover the energy consumption of the desalination unit, realizing a completely self-sufficient energy storage system. Also, compact and unitized solutions are essential in confined spaces such as an OWT, in order to allow a simple integration without substantial layout changes or additional offshore platforms.

## 2. Material and methods

The methodology used is this work aims to verify the coupling of the proposed system architecture. Additionally, working in a confined space it is important to estimate the possible required footprint/volumes to host the various components (e.g. rSOC, the hydrogen storage and the water desalination system) at the single turbine level.

The input anemometric data, as well as the calibration data of some component models (OWT, rSOC) presented during this work are based on real data.

Additionally, information regarding the different systems costs are given to evaluate the economic feasibility of such strategy.

### 2.1. The offshore wind farm

In this study, the case study of an existing offshore wind farm installed in Sweden is analysed, more precisely the wind farm is located in Lillgrund, in the Baltic Sea, 6 km from Malmö coastline, and it is represented in Fig. 2 (Majidi Nezhad et al., 2021).

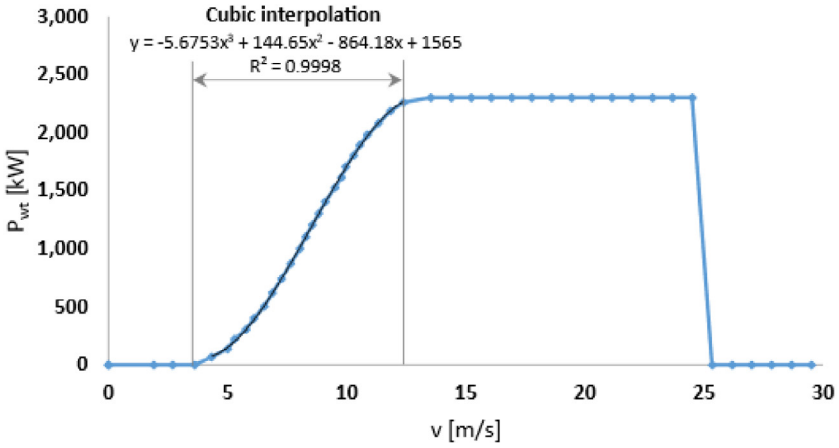


**Fig. 3.** Siemens Siemens SWT-2.3–93 power curve.

**Table 1**
Siemens SWT-2.3-93 specifics.

| | |
|---|---|
| Generator | Asynchronous; 690 [V] |
| Nominal power | 2,300 [kW] |
| Rotor diameter | 93 [m] |
| Swept Area | 6,800 [$m^2$] |
| Hub height | 65 [m] |
| SCADA system | Web WPS |
| Auxiliaries | 0.7% Nominal power (ca. 16.1 kW) |
| Cut-in wind | 4 [m/s] |
| Nominal power | 13–14 [m/s] |
| Cut-out wind speed | 25 [m/s] |

**Table 2**
Substation electrical systems.

| Electrical system | |
|---|---|
| Main transformer | 138/33 kV, 120 MVA |
| Local transformer | 33/0.4 kV, 150 kVA |
| Feeder switchgear | 33 kV |
| Local switchgear | 0.4 kV |
| Diesel backup | 110 kVA |
| Control systems | |
| Monitoring | |
| Mechanical vibration and collision | |

The farm is composed by 48 Siemens SWT-2.3–93 offshore wind turbines (Göçmen and Giebel, 2016), whose specifications are reported in Table 1 and the power curve is reported in Figure33, this latter extrapolated from the manufacturer specifications (Siemens, 2009).

The OWTs foundations are gravity based (Jesson et al., 2008), in the process was fundamental considering water depth, wave conditions and wind resource (Wu et al., 2019) to arrive to an optimal solution.

From the SCADA databases, it was possible to obtain yearly anemometric data for a period of approximately one year, starting from the 1st of July 2018 until 14th of June 2019, with a time resolution of 10 min.

In Table 1, the average auxiliary system consumption is reported, which is mainly due to navigation lights, sensor monitoring, communication systems, ventilation and heating appliances and safety systems (Merkay, 2018).

The electrical power $P_{wt}$ produced by one turbine can be deduced by applying the interpolated wind turbine power curve, reported in Fig. 1, as a piecewise expression as a function of wind speed ($v$) (Feroldi et al., 2013) – Eq. (1) – considering as breakpoints the characteristic wind speeds reported in Table 1. Since the wind speed readings are done at hub height, shear factor correction is not required for altitude.

Power losses due to wind direction variation and turbulence effects are neglected in a preliminary stage, air conditions are considered at 15 °C; 1 bar; 1.225 kg/$m^3$.

Nonetheless, a primary level control is done on the start-up and cut-off turbine periods, while a second level is performed between 12 and 25 m/s, in the nominal power region. Eq. (1) summarize the formulas used at the wind speed variations, in order to control the OWT producibility (Ali Sha et al., 2021) (see Fig. 3).

$$P_{wt}(v) = \cdots = \begin{cases} 0; & v < v_{ci} \\ a_3 v^3 + a_2 v^2 + a_1 v + a_0; & v_{ci} < v < v_{np} \\ P_{wt,np}; & v_{np} < v < v_{co} \\ 0; & v > v_{co} \end{cases} \quad (1)$$

where $v_{ci}$ and $v_{co}$ are the cut-in and cut-out wind speed respectively, while $v_{np}$ is nominal power wind speed and $P_{wt,np}$ is the related wind turbine nominal power.

The Annual Energy Production (AEP) of the OWT is calculated as the integral sum over the simulation period of the power in each timestep (obtained from the power curve interpolation) multiplied by the timestep duration.

Considering the internal grid, it is made by 5 feeders of 33 kV, for a total extension of 22 km, all connected to the same substation which is 9 km (7 offshore and 2 onshore) away from the delivery point. The substation components are described by (Jesson et al., 2008) and summarized in Table 2.

In case of emergency, considering an average diesel backup generator power factor of 0.8 and considering that the OWT auxiliaries nominal power demand is approximately 16 kW, the available diesel genset could be sufficient to supply the auxiliaries of 5 OWTs

### 2.2. The rSOC module

A rSOC module is modelled based on literature (Hauch et al., 2021; Nechache and Hody, 2019), considering the experimental efficiency for a rSOC stack (25 cells × 100 $cm^2$ unit cell active surface) at T = 700 °C. Stack tests are reported for both SOFC operation (pure $H_2$) and SOEC operation (90/10% $H_2O/H_2$, to maintain a reducing atmosphere at the fuel electrode). SOFC operation is analysed between 0.1–0.3 A/$cm^2$ with a Fuel Utilization Factor ($UF_f$) between 50%–67% while SOEC operation data is given for current densities between 0.25–0.5 A/$cm^2$ and Steam

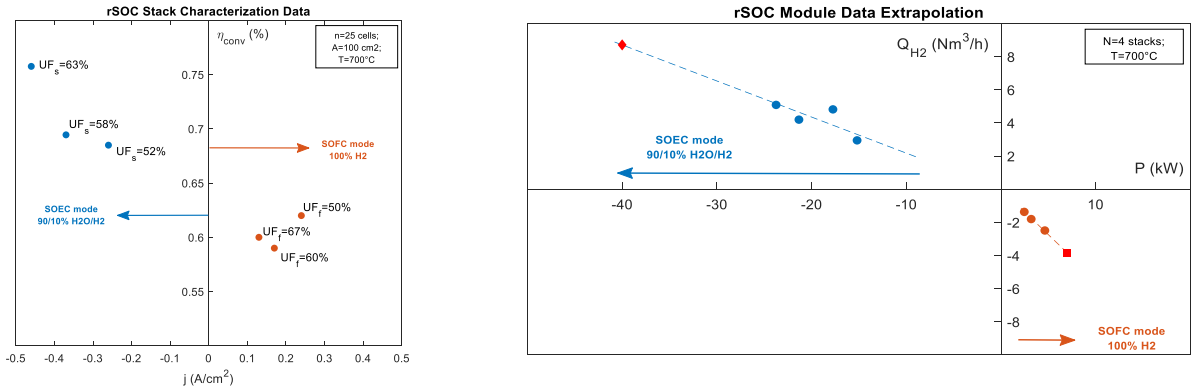


**Fig. 4.** (a) rSOC stack experimental data; (b) rSOC module characteristic curve extrapolation (41 $kW_e$ SOEC; 7 $kW_e$ SOFC).

Utilization Factors ($UF_s$) between 52%–58%. Although higher current density and reactant Utilization Factors could technically be obtained (especially in SOEC mode), the available experimental data was limited to such values due to limitations of the used test bench (Reichholf et al., 2020). The performances can be considered representative of a generalized rSOC stack, presenting comparable SOEC/SOFC capacity ratios ($P_{SOEC,nom}/P_{SOFC,nom} = 5.8$) and conversion efficiencies (around 70% in SOEC mode and 60% in SOFC mode) with respect to other systems described in literature (Buffo et al., 2020). The stack performances (in terms of power and hydrogen production/consumption) are reported in Fig. 4a.

Subsequently, the stack data is extended to the module level, considering an assembly of 4 stacks connected in series. As a first approximation, the module performance curves are obtained from a linear interpolation of the stack data (Fig. 4b) in both operating modes, up to the nominal design conditions of 40 $kW_e$ SOEC/7 $kW_e$ SOFC. The hydrogen consumption in SOFC mode is related to the hydrogen flow rate provided as an input to the rSOC module, thus implicitly considering the once-through $UF_f$ and off-gas recirculation are phenomena occurring internally the rSOC module itself. The power modulation capacity in SOEC mode is considered possible between the range 9–41 $kW_e$, producing between 2–8 $Nm^3/h$ of $H_2$. In SOFC mode, load modulation is possible between 2–7 $kW_e$, consuming between 1–4 $Nm^3/h$ of $H_2$.

In both operating modes a thermal power of 4 $kW_{th}$ at 90 °C can be recovered from the rSOC system at nominal conditions (Lamagna et al., 2021). The heat output at partial loads (both SOEC and SOFC mode) can be considered directly proportional with the load factor.

The rSOC footprint can vary between models, but it can be considered in a range varying from 0.1 $m^3/kW$ to 0.3 $m^3/kW$, according to lab-scale (Peters et al., 2021) or commercial (Solid Power, 2021) modules, respectively. Its specific capital expenditure (CAPEX) for the entire system, as inferable from Peterson (2020), is estimated in 1800 €/kW considering the FC power, with an annual operation and maintenance annual expenditure (O&M) equals to $4\%_{CAPEX}$/year. The reported cost is expected to be reached in 2030 since nowadays no commercial large-scale rSOC is available on the market (except for prototype systems). An estimation of the current cost for a prototypal system could be around 2300 €/$kW_{FC}$. Given uncertainties around the long-term prevision on the technology development, this latter value is used for the economic evaluation as a conservative approach.

### 2.3. The desalination unit

Desalination technologies can be generally divided in two main process groups: thermal and membrane. In first category are allocated the Multi-Stage Flash (MFS) (Yanan et al., 2021), and the Multi Effect Distillation (MED) (Signorato et al., 2020), while the second is dominated by the Reverse Osmosis (RO) processes (Shengnan et al., 2022). The main technical characteristics of the desalination technologies are summarized in Table 3.

Even though RO due to its high electric efficiency is the most used solution, the distillation methods can produce higher purity water and do not need of extensive pre-treatment unit (Ghaffour et al., 2013). Thermal processes can be performed at ambient pressure and a temperature between 70 °C to 120 °C, obtained by process heat or ohmic heating (Elsaid et al., 2020), or at lower temperatures at partial vacuum pressures (Assiry et al., 2010). Nonetheless, the RO has the highest Water Recovery Rate (WRR) (2) (Kim and Hong, 2018), followed by the MSF (Altaee and Zaragoza, 2014) and MED (Altaee et al., 2014) which have comparable values.

$$\text{WRR} = \textit{Permeate water Flow rate/Feed water flow rate}\ [\%] \quad (2)$$

Among the thermal processes, MED has its strengths in the low electrical energy consumption, low operation cost and high thermal efficiency (Wang et al., 2011). Moreover, MED has a greater flexibility at partial load than the MSF (García-Rodríguez, 2003) and it can be used at smaller scale (Liponi et al., 2020). Although thermal driven desalination systems are typically deployed at large-scale with a centralized approach, few studies in literature have demonstrated (also experimentally) small-scale thermal desalination systems coupled to u-CHP units of comparable scale (150 L/day with a 5 $kW_{th}$ heat input at 50 °C) (Cioccolanti et al., 2016).

To assess the thermal integration of the high-grade heat available from the rSOC with the desalination processes, the analysis is focused on the thermal-driven technologies. In particular, the MED process is chosen due to previously mentioned considerations.

Single effect MED has a footprint evaluable in 0.004 $m^3/(L/day)$ considering the purified water (Cioccolanti et al., 2015).

Despite thermal desalination processes achieve high quality permeate water, in the order of 100–1000 ppm salinity; electrical conductivity 10–100 μS/cm (Guler et al., 2010), it may not be of sufficient purity to be sent directly to the electrolysis stack, which typically operate on demineralized-grade water or steam, with a conductivity <1 μS/m. Although the higher temperature and ceramic materials in the SOEC lead to a lesser susceptibility to water quality, with some studies even reporting stable performances with direct seawater feed to the SOEC stack (Baldinelli et al., 2020), the conservative assumption of a purification step is considered, with an in-built demineralization system included in the SOEC balance of plant. The demineralization system is typically based on electricity-driven membrane technology (RO) with a WRR of around 50%.

**Table 3**
Desalination technologies comparison summary.

| Process | Thermal energy [kWh/m$^3$] | Electrical energy [kWh/m$^3$] | Total energy [kWh/m$^3$] | WRR [%] | CAPEX [$/m$^3$d] |
|---|---|---|---|---|---|
| MSF | 7.5–12 | 2.5–4 | 10–16 | 33 | 1200–2500 |
| MED | 4–7 | 1.5–2 | 5.5–9 | 32 | 900–2000 |
| RO | 0 | 3–4 | 3–4 | 50 | 900–2500 |

Therefore, the total water mass balance should consider the various steps of pre-treatment (desalination + demineralization) to determine the total input seawater and total energy consumption in the integrated system. In the analysed case (MED + RO), the global WRR (as ratio between demineralized water fed to the SOEC stack and input seawater) is equal to 16%. Instead, the electricity demand of the demineralization system is not seen as an additional energy consumption (included in SOEC balance of plant consumption). For the economical evaluation, the cost of 2500 $/m$^3$ day is assumed for the water treatment system and 4% $_{CAPEX}$/year is considered for the annual O&M

### 2.4. Compressor and storage

The rSOC module is complemented by a compressed gaseous hydrogen ($CGH_2$) storage system which processes the produced hydrogen in SOEC mode. The storage system is composed of (i) a hydrogen compressor (typically reciprocal) and (ii) a pressure-controlled compressed hydrogen storage tank. Since both systems present high levels of technology maturity, the design parameters (flow rate, pressure, and storage capacity) can be easily tailored for the case-specific application, in relation to the SOEC hydrogen production capacity.

The hydrogen compressor specific energy consumption (kWh/Nm$^3$) is calculated as a function of the pressure ratio $\beta$ assuming an isentropic transformation, with 65% and 93% of isentropic and electric efficiency respectively, considering thermodynamic properties at the average gas temperature via the thermodynamic library CoolProp (Gallardo et al., 2020). The compressor size is determined by multiplying the Specific Energy Consumption (SEC) by the maximum hydrogen production flow ($QH_{2PMax}$) in SOEC mode, obtaining the nominal power of the compressor (3).

$$P_{comp} = SEC * Q_{H2,PMax}\ [kW] \tag{3}$$

The compressor cost is assumed according to Reußet al. (2017) with an overall specific CAPEX and annual OPEX of 3900 $/kW and 4% $_{CAPEX}$/year, respectively.

The hydrogen storage is modelled under the assumption of ideal gas conditions (which is acceptable for gas pressures below 1000 bar), therefore the tank pressure is directly linked to the mass balance in the storage volume (Monforti Ferrario et al., 2020). The State of Charge (SOC) of the storage tank is given by the ratio of the operating pressure (bar) respect to the nominal pressure (bar). The sizing of the storage section is performed by analysing the temporal interval between non-producibility events and the time distribution of the non-producibility events. As a precautionary assumption the storage tank is sized to guarantee the stand-alone operation of the rSOC storage system (i.e. zero external energy required from feeder) considering the storage tank is initially full (SOC = 100%). The hydrogen tank CAPEX is taken as 338 $/kg$H_2$ (Ikäheimo et al., 2018) and 4% $_{CAPEX}$/year to gauge the annual O&M.

### 2.5. Integrated system modelling

The integrated system can be schematized as shown in Fig. 5. The main system objective is to minimize or eliminate the back-feed from the underwater cable during the OWT downtime.

The integrated system modelling is carried out in MATLAB/Simulink environment (Fig. 6a), where each component is represented as a black-box input/output model which are subsequently integrated in a system level block diagram. Each model component elaborates the input vectors (energy or mass) according to the conversion characteristics described in the previous sections. The mass/energy balance equations are solved determining the operating conditions of the integrated system at each timestep (10-minute interval).

The programmable components (rSOC) are operated according to a control system which provides the selected operation mode signal (SOFC/SOEC) mode according to a rule-based logic. The definition of the rule-based control logic is defined by global user-defined strategies (e.g. guarantee of supply of auxiliary demand, minimization of external energy supply, maximization of hydrogen production, etc.)

A rule-based control logic (Fig. 6b) is implemented in the Energy Management System (EMS) block via case structured programming, driven by $P_{wt}$ and controlled by the SOC of the hydrogen storage tank. A minimum SOC equal to 10% is implemented for safety reasons and to avoid complete emptying of the tank (Cau et al., 2014). Two different global strategies over the rSOC have been implemented: one dedicated only to the auxiliary demand coverage; another with the possibility to continuously produce hydrogen from the OWT electricity for exportation purposes. In both strategies the system is operated to completely avoid external energy from the backfeeder. The two control strategies are reported in detail as follows.

#### 2.5.1. Scenario 1 — Auxiliary demand coverage strategy

Scenario 1 is based on the concept that the rSOC is only dedicated to the OWT auxiliary systems, it will operate the rSOC system only to the extent strictly required by the demand, prioritizing the replenishing of the storage tank and avoiding unnecessary usage. Consequently, the utilization factor of all storage components is reduced, following the rSOC requirements.

In the case that $P_{wt}$ is null – i.e. OWT is not producing electricity for wind speed beyond the operating ranges or for maintenance – if the SOC of the tank is greater than 10%, the auxiliary system demand is covered by the rSOC in SOFC mode (therefore consuming $H_2$ thus emptying the tank), otherwise (if the SOC is in a critical low level) the auxiliary demand is covered by the feeder. In case of positive $P_{wt}$ – OWT running – electricity is converted to hydrogen in SOEC mode to replenish the tank until a SOC value of 90% is reached. Above this value the rSOC is disconnected and no storage service is provided to the wind turbine, which fully evacuates the produced power through the underwater cable towards the mainland electrical substation.

The SOEC operational profile determines the water demand, which subsequently defines the MED operational profile. The electricity required by the desalination system is sourced from the OWT.

#### 2.5.2. Scenario 2 — Hydrogen export strategy

Scenario 2 is an extension of Scenario 1, with the addition of the possibility to continue producing hydrogen in SOEC mode beyond the 90% tank SOC threshold, which could subsequently be sold and exported elsewhere. In this way, the implementation

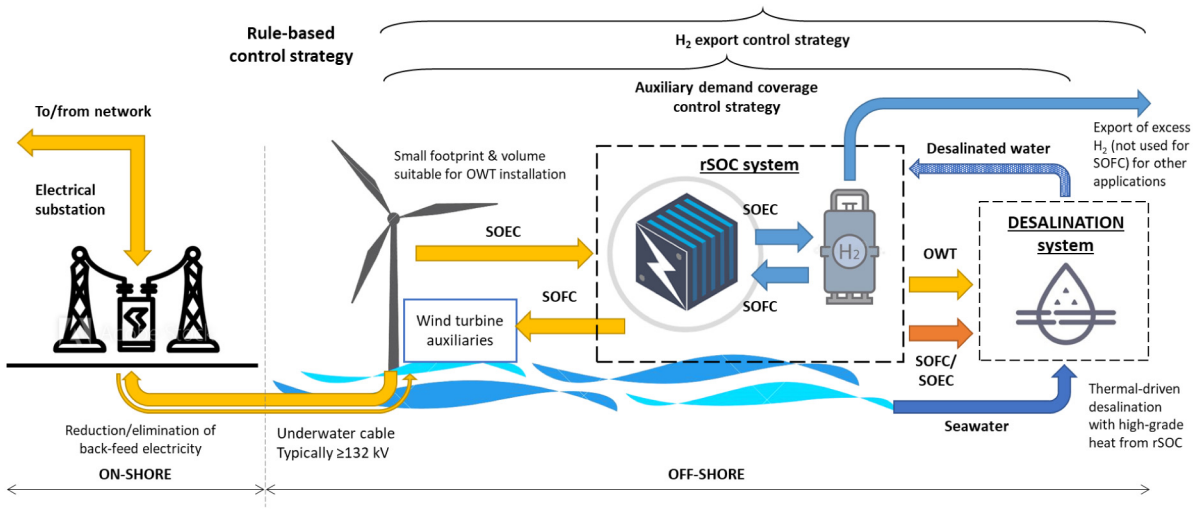


**Fig. 5.** Scheme of the integrated OWT + rSOC system.

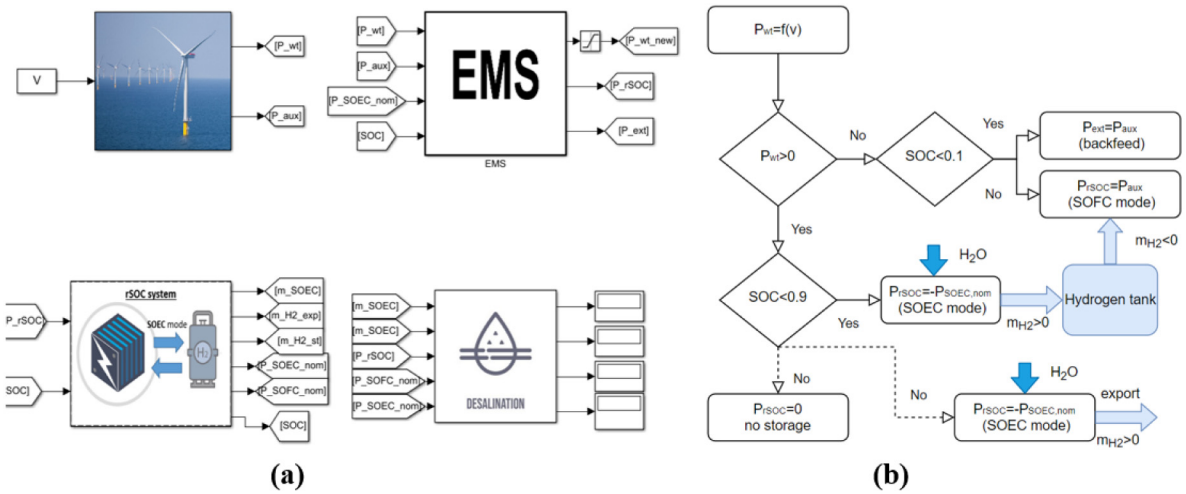


**Fig. 6.** (a) Scheme of integrated system model in Simulink environment; (b) flowsheet of the implemented rule-based control logic.

of a rSOC coupled to the OWT is seen as not only a UPS for the auxiliary systems, but also as a hydrogen generator when it is not required to cover the auxiliary demand. Scenario 2 aims to maximize the overall utilization factor of the rSOC (especially for what regards SOEC mode), drastically increasing the hydrogen production amount. The hydrogen export stream is preliminarily considered to be evacuated continuously, since the hydrogen transport is out of the scope of this research. Assumed

The logical structure is the same as Scenario 1, with the addition of SOEC operation when SOC has reached 90%. The feeder use is allowed to cover the auxiliary demand only in critical conditions, i.e. the tank SOC below 10%.

Since the desalination profile follows the SOEC profile, also the water demand and subsequent water treatment demand will be drastically increased, with respect to Scenario 1. As for Scenario 1, the electricity required by the desalination system is sourced from the OWT.

Then, to transport the produced hydrogen towards the mainland, a system of subsea pipelines is assumed. Indeed, to construct such an infrastructure for only one OWT will be too expensive, hence the production of the entire farm will be considered. To assess the pipelines length, the pipelines are assumed to be installed parallelly to the electric cables, for a total length of 31 km and with a CAPEX of 400 $/m at 150 bar (Crivellari and Cozzani, 2020). Since the transmission pressure is lower than compression and storage working pressure, no additional work is required to send the gas stream to the receiving point. Additionally, an annual O&M of $4\%_{capex}$ is assumed for operation and maintenance.

**Table 4**
PMT formula components and assumptions.

| Component | Scenario 1 | Scenario 2 |
|---|---|---|
| r, Annual interest rate | 5.12% | |
| n, Years of payments | 20 | |
| p, Loan (total CAPEX + OPEX) [$] | 101,662 | 18,408,570 |
| PMT [$/year] | 8,240 | 1,492,218 |

### 2.6. Economic analysis

A project financing economic model is used to address the expenses, evaluating the periodic payment for an annuity (PMT) described in Eq. (4), with the assumption resumed in Table 4.

$$PMT = P * \frac{r}{1 - \left(\frac{1}{(1+r)^n}\right)} \ [\$] \tag{4}$$

It is worth noting that the main difference between the two scenarios is due to the pipeline installation, moreover, scenario 1

can be seen as the economic assessment of the storage system at single OWT level, while scenario 2 considers the same system but at wind farm level, plus the distribution system to the mainland.

Considering the hydrogen production in the two scenarios, is possible to estimate the Levelized Cost of Hydrogen (LCOH) dividing the PMT for the total annual hydrogen production, as reported in formula (5):

$$LCOH = PMT/H2_{prod,SOEC}\ [\$/kg_{H2}] \quad (5)$$

The LCOH is key to understand if the hydrogen produced in loco is cost competitive with other external solutions.

Similarly, the Levelized Cost of Storage (LCOS) can be obtained considering the energy supplied to the auxiliaries, as reported in Eq. (6):

$$LCOS = PMT/E_{prod,SOFC}\ [\$/MWh] \quad (6)$$

The LOCS will simplify the comparison process with other storage systems such as the diesel back-up generator or Li-Ion batteries, mostly used in those cases, to understand how this solution can be competitive.

### 2.7. Key Performance Indicators (KPI)

The system is simulated under both control strategies and the results are assessed from an integrated analysis standpoint via several Key Performance Indicators (KPI) such as: energy production of the OWT (GWh), total energy to the auxiliary systems (MWh), SOFC energy production ($MWh_e$), percentage repartition (%) of energy supply to the auxiliaries between the SOFC and the feeder, SOEC energy consumption ($MWh_e$), SOEC total produced hydrogen quantity (kg) and percentage repartition (%) between local storage and export, utilization factor of the rSOC in SOFC and SOEC mode (%), MED electrical/thermal energy consumptions ($MWh_e$; $MWh_{th}$), average hydrogen storage tank pressure (bar) and average hydrogen storage tank SOC (%). From the economical point of view, LCOH and LCOS will be evaluated as KPIs to compare the proposed system with the other solutions available on the market.

## 3. Results

In this section the simulation results and obtained KPI values will be presented. The results are collected and divided in two sections, one referred to the OWT production, what can be considered the *ex-ante* scenario, and a second referred to the new proposed system, where the comparison of the two considered scenarios according to the rSOC control strategy are reported.

### 3.1. Wind farm production and auxiliary systems' energy demand assessment: ex-ante scenario

The analysis of the performance of the OWT in the ex-ante scenario (no storage) allows to provide a benchmark for the system KPIs and is key to understand the stochastic electricity production from the wind resource. In particular, turbines B8 and D8 are analysed, for which a full anemometric dataset is available for the whole analysed period without gaps in the data.

The wind data profile (Fig. 7a) shows as most frequent wind speed the range between $v_{ci}$ and $v_{np}$. The average wind speed is in the range of 7–8 m/s while the range $v_{np}$ and $v_{np}$ is less frequent. Wind speeds above $v_{np}$ are very rare and occur only on few occasions throughout the year. Fig. 7b shows the wind direction distribution, in relation to its speed intensity. However, as a first approximation it is considered that the OWT yaw and pitch modulation systems can fully exploit the available wind resource in every direction. As shown in Fig. 7c, the wind speed distribution determines that the OWT mostly operates in the wind curve cubic region and, to some extent, at nominal power (2.3 MW). The AEP is around 8.3–8.5 GWh (Fig. 7d), resulting in a capacity factor close to 42% which is a typical value for offshore wind in favourable locations such as the Nordic Sea (IEA, 2019a; Jacobsson and Karltorp, 2013).

The auxiliary demand profile directly follows the producibility data of the OWT (Fig. 7e), appearing in the instances where $P_{wt}$ is equal to zero when the wind speeds are below cut-in or above cut-out. The annual energy consumption related to the auxiliaries which is not supplied by the turbine, and therefore must be supplied entirely by the feeder in the ex-ante scenario, is equal to 20.55 MWh (Fig. 7f). This amount represents only 0.2% of the OWT AEP, showing a wide difference between both the nominal power of the OWT and the auxiliary systems and the annual energy demand.

### 3.2. Integrated system results

For the new proposed scenarios, the study is focused on the coupling to a single turbine. The simulations are carried out in Simulink environment with fixed 10-minute timestep intervals (based on the available anemometric data resolution), resulting in 52,560 timesteps for a yearly simulation and they will be carried out the two control strategies.

Since the compressor is strictly connected with the rSOC operation, the compressor sizing and operation can be derived from said operational profile. Given the integrated system mass/energy balance, it will be possible to appropriately design the compression and storage. This information will be collected in the final section to provide a complete overview of the design and operation of the whole integrated system.

#### 3.2.1. Design parameters definition: rSOC and MED

Considering the auxiliary power demand of 16.1 $kW_e$ (0.7% of the 2.3 $MW_e$ OWT), three rSOC modules are required to cover the demand power in SOFC mode, resulting in a SOFC power of 21 $kW_e$ in SOFC mode operating at around 75% of load modulation.

Considering the $UF_f$ and recirculation which occurs internally to the rSOC system itself, the estimated hydrogen consumption is around 8.8 $Nm^3/h$, which is obtained from the stack-to-module data extrapolation (described in Section 2.2). The same rSOC system can be operated in SOEC mode with a maximum input power of 122.4 $kW_e$, producing up to 26.6 $Nm^3/h$ of hydrogen. In both operating modes, the thermal power related to the excess heat is between 9–12 $kW_{th}$.

The maximum SOEC demineralized water requirement is equal to around 23.8 L/h, related to the rated hydrogen production capacity in SOEC mode (26.6 $Nm^3/h$ at nominal power), leading to a maximum seawater requirement of around 150 L/h (0.15 $m^3/h$) according to the global WRR (considering both desalination and demineralization units). Assuming continuous operation as worst-case assumption, the aggregate daily water treatment of the MED system is equal to 3.5 $m^3$/day. Considering its rated capacity, the input thermal and electrical and power demand to the MED system are equal to 0.6–1.1 $kW_{th}$ and 0.2–0.3 $kW_e$ respectively. In Table 5 the main design parameters of the rSOC and MED systems are reported.

The total encumbrance, considering the footprints presented in Section 2, for the system made of the rSOC and the MED system is slightly below 20 $m^3$.

#### 3.2.2. Operational parameters: rSOC and MED

The dynamic operation results of the rSOC + MED integrated system for the analysed period (1 year) under the two control strategies are presented and discussed, considering the nominal design parameters reported in Table 5.

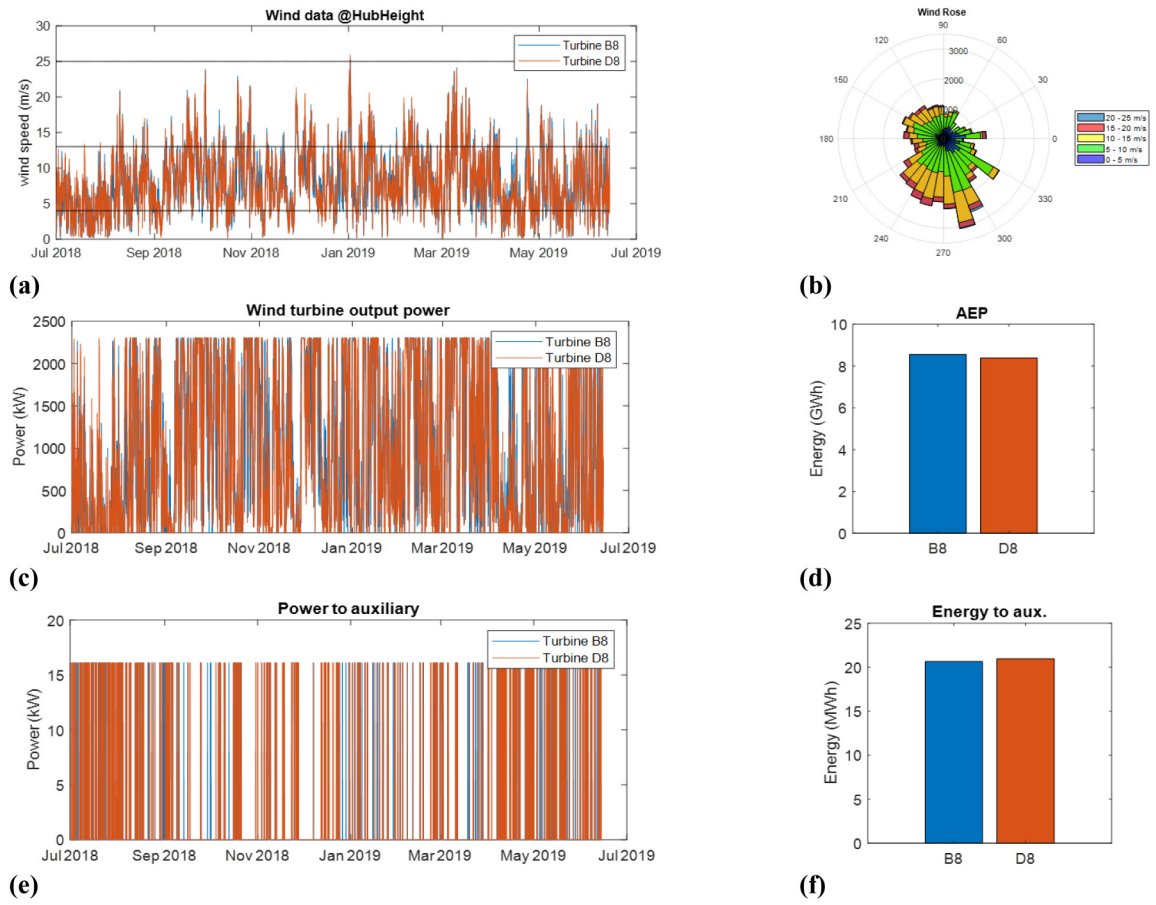


**Fig. 7.** Ex-ante simulation results for OWT B8 and D8 for the analysed period: (a) anemometric wind speed data at hub height respect to $v_{ci}$, $v_{np}$, $v_{co}$ (solid black lines); (b) wind rose for B8; (c) OWT power production profile; (d) OWT Annual Energy Production; (e) auxiliary power demand profile; (f) auxiliary energy consumption (when not supplied by the OWT).

**Table 5**
rSOC and MED nominal design parameters.

| Design parameter | Unit | Value |
|---|---|---|
| **rSOC system** | | |
| Number of modules | [#] | 3 |
| Geometrical volume | [$m^3$] | 5.5 |
| rSOC thermal output (SOFC/SOEC) | [$kW_{th}$] | 12 |
| rSOC global WRR | [%] | 16% |
| **rSOC (SOEC) system** | | |
| SOEC nominal power | [$kW_e$] | 123 |
| SOEC nominal hydrogen production capacity | [$Nm^3$/h–kg/h] | 26.6–2.39 |
| SOEC average conversion efficiency | [%] | 71% |
| SOEC demineralization WRR | [%] | 50% |
| **rSOC (SOFC) system** | | |
| SOFC nominal power | [$kW_e$] | 21 |
| SOFC nominal hydrogen consumption capacity | [$Nm^3$/h–kg/h] | 11.5–1.03 |
| SOFC average conversion efficiency | [%] | 60% |
| **Desalination (MED) system** | | |
| MED nominal seawater treatment capacity | [L/h–$m^3$/day] | 150–3.5 |
| MED WRR | [%] | 32% |
| MED nominal power demand | [$kW_e$–$kW_{th}$] | 0.3–1.05 |
| Geometrical volume | [$m^3$] | 14 |

*3.2.2.1. Operational results: Scenario 1.* In Fig. 8 the operational results and aggregate energy balances of the integrated system under the auxiliary demand coverage control strategy (Scenario 1) are reported. The rSOC system is operated in SOFC mode for 1,283.8 h to supply the auxiliary systems' demand (equal to the OWT downtime periods reported in Section 3.1) and in SOEC mode for 424.5 h to replenish the storage tank according to the control strategy. The rSOC profile follows an on–off trend, switching between SOFC and SOEC mode, given the structure of the control logic and the relative sizing of the components.

The whole energy demand of the auxiliary systems (20.55 MWh) is covered in SOFC mode (SOFC utilization factor 11.7%). A total energy 52.59 MWh is consumed in SOEC mode (SOEC utilization factor 5.14%) which is deduced from the OWT energy production which is reduced by 0.5% from 8.55 GWh to 8.51 GWh, producing 1029 kg which is entirely sent to the storage unit for local demand management. The desalination energy consumptions are very low, 0.13 $MWh_e$ and 0.45 $MWh_{th}$, given the limited amount of water required in SOEC mode (10.51 $m^3$ demineralized water input to the SOEC unit; 64.43 $m^3$ input seawater to the MED unit). As previously discussed, the electrical/thermal energy consumptions of the MED system are almost negligible in relation to the global energy balance.

*3.2.2.2. Operational results: Scenario 2.* The operational results and aggregate energy balances under Scenario 2 control strategy shown in Fig. 9 clearly show a dramatic increase in the SOEC utilization (7078 h) in nominal conditions for hydrogen production. In fact, the SOEC utilization factor is increase to 84.73%, consuming 867.1 MWh which causes a large increase in hydrogen production (16,960 kg), of which only around 6% is sent to the storage (1029 kg, similarly to Scenario 1), while the remaining 94% (15,931 kg) is sent to export. The increased SOEC energy consumption is at expense of the OWT energy production, which is reduced more significantly than in Scenario 1 (9.82% reduction, down to 7.71 GWh). Considering that the SOFC operation is unchanged (1282.8 h; SOFC utilization factor 11.7%), the total

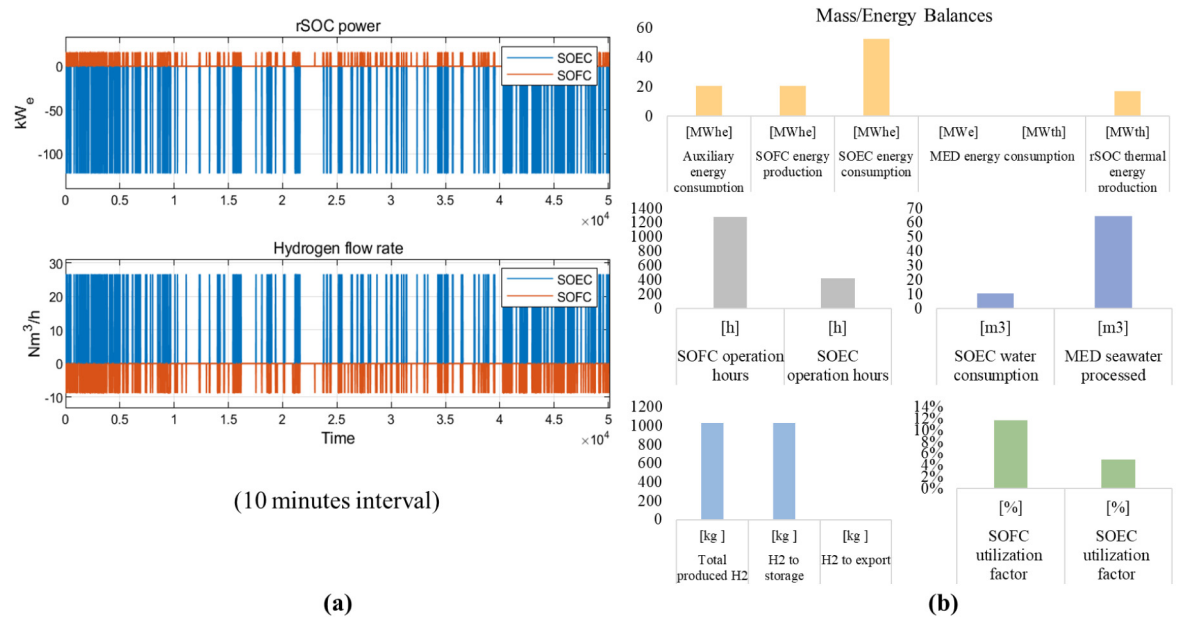


**Fig. 8.** Simulation results for Scenario 1 — (a) rSOC dynamic response; (b) aggregated mass/energy balances.

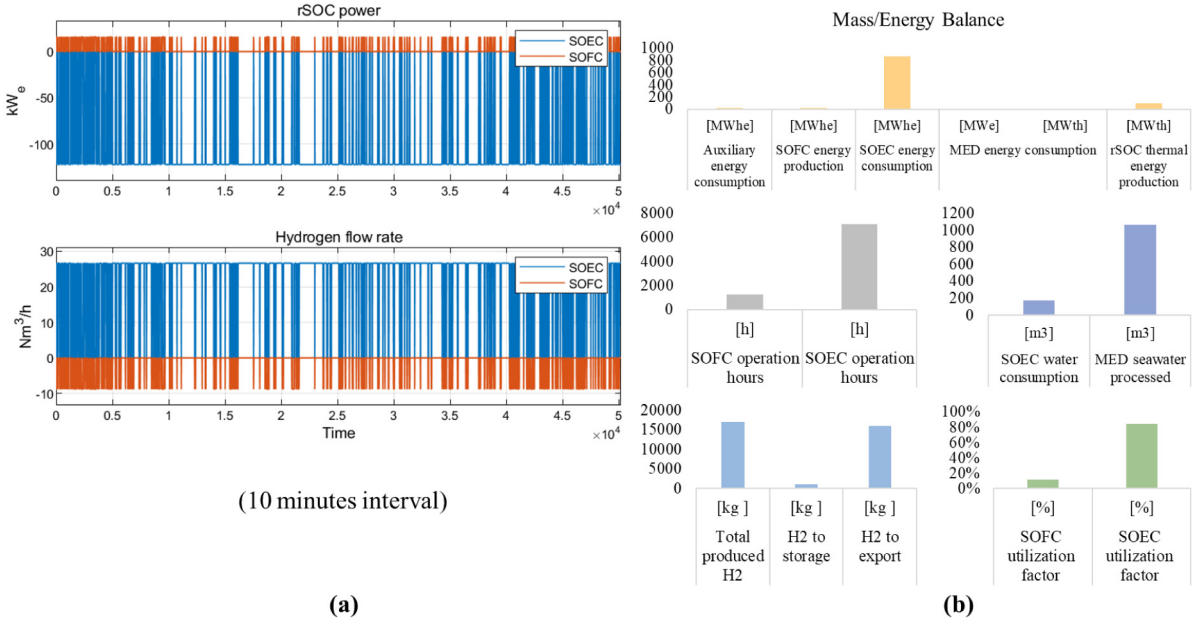


**Fig. 9.** Simulation results for Scenario 2 — (a) rSOC dynamic response; (b) aggregated mass/energy balances.

rSOC utilization factor is increased (96.44% respect to 16.72% in Scenario 1) due to the increase of utilization in SOEC mode. Even though the total water is increased (169.92 $m^3$ demineralized water input to the SOEC unit; 1062 $m^3$ input seawater to the MED unit) as a consequence of the increased hydrogen production, the aggregate MED energy consumption remains quite low (2.13 $MWh_e$ and 7.44 $MWh_{th}$) respect to the overall energy balance of the integrated system. Furthermore, the rSOC thermal output (96.75 $MWh_{th}$) is still widely compatible with the MED thermal energy demand, also due to the increased rSOC utilization which leads to more excess heat production.

*3.2.2.3. Operational results: scenario comparison.* In Fig. 10 the normalized results in terms of KPIs (OWT energy production, desalination total energy consumption, produced $H_2$, and rSOC utilization factor) are provided to illustrate the operation results according to the control logic. Scenario 1 presents low normalized values of $H_2$ production, rSOC utilization and consequently, desalination energy demand.

*3.2.3. Design & operational parameters: compression and storage*

Although the compressor energy demand is included in the SOEC energy consumption (reported in Fig. 4) its calculation is necessary to correctly size the compressor component. Although the electricity consumption of the compressor is a function of the hydrogen tank pressure (variable outlet pressure) a worst-case scenario (1–180 bar) has been considered, leading to a specific electrical energy consumption of 2.75 $kWh_e/kg$. Considering that the maximum hydrogen production capacity of the SOEC system is around 2.5 kg/h, the compressor nominal power is equal to approximately 7 $kW_e$. Commercially available compressors are sold with determined characteristic in terms of charging rate,

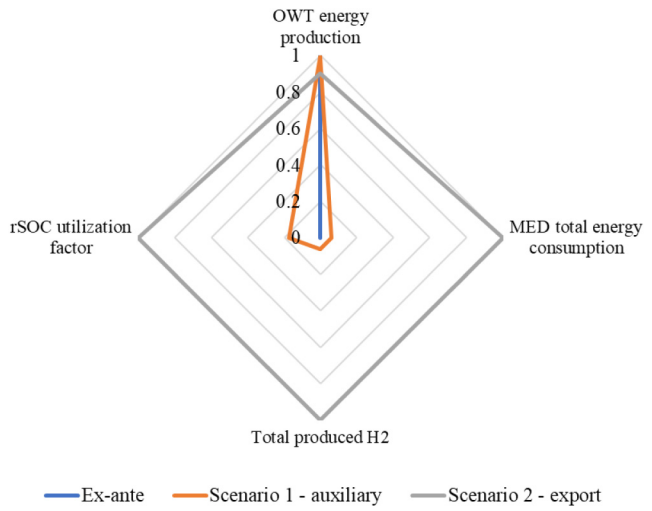


**Fig. 10.** Normalized aggregate KPIs from the integrated system simulations.

pressure, and dimensions. Nevertheless, thanks to the fixed storage pressure it is possible to individuate a product reference for this case study, which occupies approximately 0.5 $m^3$ as tested in Bauer kompressoren (2021).

With respect to the hydrogen storage tank, it must be sized in close relation to the operation phase, in order to complete stand-alone operation and avoid all external energy input from the feeder (SOC $>$ 10% for the whole simulation period). In Fig. 11, a statistical analysis of the non-producibility duration and intervals is reported. The maximum non-producibility duration (164 timesteps; 1640 min) represents the minimum requirement for the storage sizing. Also other aspects must be considered such as the time interval between non-producibility events, restrictions in SOC operating ranges stated at 10% as minimum and 90% as maximum, and the possibility that the actual SOC value during a non-producibility event might be lower due to prior non-producibility events. Taken all aspects into consideration, the storage was sized by iterative simulation. The minimum storage capacity value to obtain the goal is equal to 37 kg of hydrogen (1.2 $MWh_{ch}$ in the form of hydrogen – LHV equal to 33.3 $kWh_{ch}/kg$ – i.e. 740 $MWh_e$ of useful energy considering an average SOFC 60% conversion efficiency). Assumed a nominal pressure of 180 bar, this is translated into a storage tank with a geometrical volume of 2.3 $m^3$.

Since the control strategy prioritizes the tank refilling via SOEC operation, the storage pressure and SOC is generally maintained close to the upper limit. The yearly average pressure and SOC equal to 163.1 bar and 90.63%, respectively in both scenarios, except few local minimums which represent the limiting factor for the design of the storage unit as can be seen in Fig. 11. The storage sizing process is worst-case scenario driven, since low SOC conditions occur only few times during the simulation period. Nevertheless, it is preferable to oversize the hydrogen tank storage capacity to avoid external back-feed energy supply from the feeder. Tables 7 and 8 report the main design and operation parameters regarding the compression and storage systems.

Given all the incumbrance assessed, a minimum volume of 22.3 $m^3$ would be occupied by the components only, most of which is composed of the MED system. Additionally, in the case of hydrogen export, more room will be needed according to the transporting solution and the distance from the shore which determine the storage size and discharge frequency.

### 3.2.4. Economic evaluation

Finally, after the sizing of each component it is possible to evaluate the total CAPEX and the annual O&M costs, these latter are ported in Table 9.

To the O&M must be added the cost of the electricity used to produce hydrogen to obtain the total Operational Expenditure (OPEX). Considering the values of SOEC electricity consumption reported in Table 5, and the average wholesale electricity price in Sweden in 2021 of 50 $/MWh (Statista, 2022) and considering only the 35% addressable to the energy component (Vattenfall, 2022) which is considered as a lost revenue from the wind farm perspective, an electricity cost of 917 $ and 14,567 $ must be considered respectively for scenario 1 and 2.

Using formula (4) we finally obtain a total LOCH for the scenario 1 of 8.01 $/$kg_{H2}$ and 1.95 $/$kg_{H2}$ for the scenario 2.

Since the distribution pipeline cost is not part of the economic analysis for the LCOS, the analysis is only performed at single turbine level excluding the cost of the pipeline and considering the energy supplied in SOFC mode to the auxiliaries (Table 6) which resulted in a LCOS equal to 401 $/MWh using formula (5).

## 4. Discussion

With respect to the analysed wind profile, $P_{aux}$ is mostly related to low-wind conditions, rather than high wind conditions. Although the total auxiliary energy is very small respect to the AEP, the timing is indisputably relevant. In fact, external auxiliary supply during OWT down-time is required for a total of 1283 h in the analysed period (i.e. 15.34% of the total hours). Since $P_{aux}$ is several orders of magnitude lower than $P_{wt}$, the auxiliary demand presents itself as an on–off profile at its nominal load (16.1 kW) when $P_{wt}$ is null.

From the ex-ante scenario, the work continued with the two control strategies, firstly analysing in both case the possible match between the thermal demand associated to the desalination and the thermal production from the rSOC and then the coupling with the storage and compressor systems.

Since the excess heat power from the rSOC system (9 $kW_{th}$ in design operating conditions) is above the thermal power demand of the MED (0.85 $kW_{th}$ average) it can be stated that the rSOC can be coupled from a thermal point of view with the MED desalination unit.

Additionally, if the MSF process were to be considered instead of MED, the desalination thermal power demand would be slightly higher (between 1.1–1.8 $kW_{th}$) but still compatible with the rSOC excess heat power. In both cases, the desalination unit rated thermal and electric powers are quite low relatively to the other components, thus they can be neglected in the dynamic simulation since their impacts on the overall power balance is minimal.

Concerning the comparison between the scenarios, it is worth noting how the OWT energy production is barely decreased compared to the ex-ante scenario. On the other hand, Scenario 2 maximizes the rSOC utilization factor (mainly in SOEC mode) which consequently also maximizes the MED total energy demand (although still quite small relatively to the integrated system energy balance), which causes a more consistent reduction of the OWT energy production which is consumed in the electrolysis process. The introduced dedicated storage is also associated with the compression system. Considering that the first cause associated to the OWT standby can be inferred to the low wind speeds, the storage was sized accordingly. In addition, to be conservative, also other factors such as the events frequency and duration were analysed to arrive at the result, obtained by means of iterative simulations.

Given the entire system architecture, the total impact on the energy production is modest, representing less than the 10%

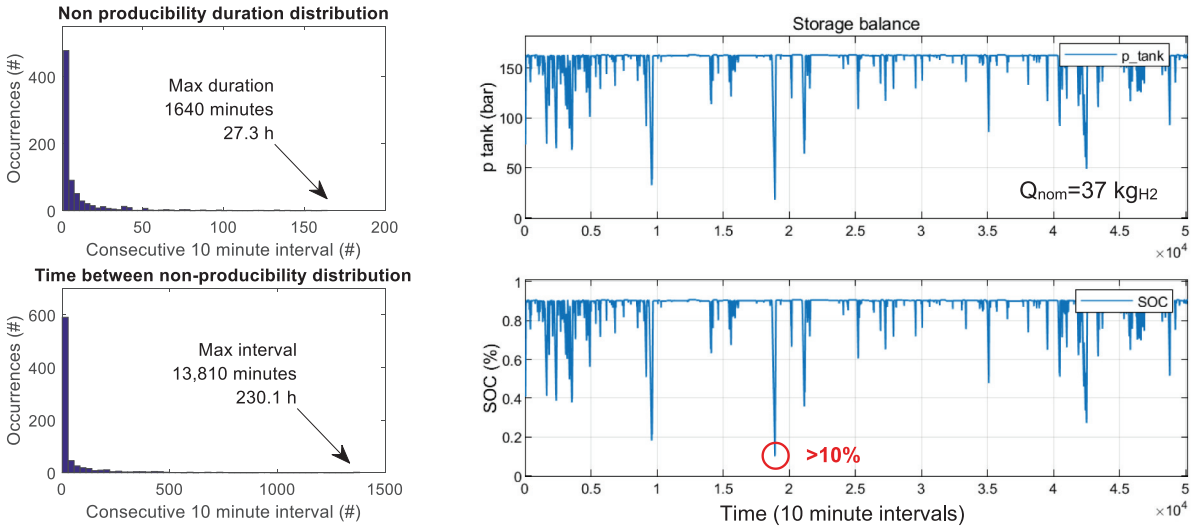


**Fig. 11.** Non-producibility statistical analysis (duration and interval) and subsequent storage sizing.

**Table 6**
Comparison of simulation results: KPIs summary.

| Operational parameter | Unit | Ex-ante | Scenario 1 | Scenario 2 |
|---|---|---|---|---|
| | | No storage; Back-feed for auxiliary | rSOC storage; Aux. demand strategy | rSOC storage; Export strategy |
| | | **Mass/Energy balance** | | |
| OWT energy production | [$GWh_e$] | 8.55 | 8.51 | 7.71 |
| Auxiliary energy consumption | [$MWh_e$] | 20.55 | 20.55 | 20.55 |
| SOFC energy production | [$MWh_e$] | – | 20.55 | 20.55 |
| SOFC operation hours | [h] | – | 1,283.8 | 1,282.8 |
| SOFC utilization factor | [%] | – | 11.70% | 11.70% |
| Auxiliary energy from SOFC | [%] | – | 100% | 100% |
| Auxiliary energy from feeder | [%] | 100% | 0% | 0% |
| SOEC energy consumption | [$MWh_e$] | – | 52.59 | 867.1 |
| SOEC operation hours | [h] | – | 424.5 | 7078 |
| SOEC utilization factor | [%] | – | 5.02% | 84.73% |
| Total produced $H_2$ | [kg] | – | 1,029 | 16,960 |
| $H_2$ to storage | [kg] | – | 1,029 | 1,029 |
| $H_2$ to export | [kg] | – | 0 | 15,931 |
| $H_2$ to storage | [%] | – | 100% | 6% |
| $H_2$ to export | [%] | – | 0% | 94% |
| SOEC water consumption | [$m^3$] | – | 10.51 | 169.92 |
| MED seawater processed | [$m^3$] | – | 64.43 | 1062 |
| MED energy consumption | [$MWh_e$] | – | 0.129 | 2.13 |
| | [$MWh_{th}$] | – | 0.451 | 7.44 |
| rSOC thermal energy production | [$MWh_{th}$] | – | 16.9 | 96.75 |
| rSOC + MED thermal compatibility | | – | Yes | Yes |

**Table 7**
Compressor and storage nominal design parameters.

| Design parameter | Unit | Value |
|---|---|---|
| **Compressor** | | |
| Compressor specific energy consumption (1–180 bar) | [$kWh_e$/kg] | 2.75 |
| Compressor nominal power | [$kW_e$] | ≈ 7 |
| Compressor geometrical volume | [$m^3$] | 0.5 |
| **Storage (compressed hydrogen storage tank)** | | |
| Maximum non-producibility event duration | [h] | (27.3) |
| Maximum interval between non-producibility events | [h] | (230.1) |
| Storage tank nominal pressure | [bar] | 180 |
| Storage tank nominal hydrogen capacity | [kg] | 37 |
| Storage tank Nominal energy capacity (full load) | [$kWh_{th}$–$kWh_e$] | [1,233–740] |
| Storage tank geometrical volume | [$m^3$] | 2.3 |

of the total production in the most demanding case (scenario 2). In terms of encumbrance, the system will require at least 22.3 $m^3$, where the MED components represents the 63% of the total. Considering the volume of 1508 $m^3$ for a 2MW OWT tower (Nabiyan et al., 2021), this is translated in less than 2%.

From an economic point of view, the installation of such a system, in a single isolated OWT, as scenario 1 shows, is similar to a Li-Ion battery CAPEX. In fact, the total CAPEX of 97 k$ obtained in scenario 1, is comparable with Li-Ion battery pack with a specific cost 237 $/kWh which would costs approximately 101k$ (Mauler

**Table 8**
Storage nominal operational parameters.

| Operational parameter | Unit | Ex-ante | Scenario 1 | Scenario 2 |
|---|---|---|---|---|
| | | No storage; Back-feed for auxiliary | rSOC storage; Aux. demand strategy | rSOC storage; Export strategy |
| | | | **Storage balance: 37 $kg_{H2}$ @ 180 bar** | |
| Storage tank average pressure | (bar) | – | 163.1 | |
| Storage tank average SOC | (%) | – | 90.63% | |

**Table 9**
System component CAPEX and OPEX.

| Component | CAPEX [$] | O&M [$] |
|---|---|---|
| rSOC | 48,300 | 1932 |
| Desalination | 8,750 | 350 |
| Compressor | 27,300 | 1,092 |
| Tank | 12,520 | 500 |
| Pipeline system[a] | 12,350,400 | 494,016 |

[a]Only for the export strategy, considered at wind farm level, all other costs are assessed at single wind turbine level.

et al., 2021) to meet an equivalent energy storage requirement of 435 kWh. Nonetheless, the battery pack could suffer the air salinity in the maritime environment, plus its discharge-recharge efficiency should considered according to the model dynamic. Considering the diesel genset, to obtain a similar performance, a 16 kW diesel generator is needed, and with a cost of 306$/kW plus a storage of 180 litres to cover the longest supply interruption period (27.3 h), a final CAPEX lower than 10k$ is obtained, representing a conspicuous cost reduction if compared with the previous options (Suman et al., 2021).

Considering now the LCOS result for the rSOC of 401 $/MWh, it is comparable with a Li-Ion battery value, which varies between 263–471 $/MWh (Lazard, 2018) and with a diesel generator for which it varies between 225–404 $/MWh (Lazard, 2014). For this latter, many other considerations must be done which can impact strongly the KPI, such as the emissions and diesel costs, and the difficulties to refill the storage in adverse operability conditions. From a resiliency point of view, if an extreme event occur (thus a longer energy demand period for the auxiliary systems) the rSOC system would be able to supply the demand in SOFC mode for around 46.8 h considering a full hydrogen tank (37 kg, according to the selected design which is not based on extreme events) and the hydrogen consumption of the SOFC in the demand conditions (16 kW, consuming around 0.79 kg/h with a efficiency of around 61%). Moreover, the rSOC system is also able to locally produce additional hydrogen in SOEC mode to possibly increase even further the autonomy in extreme conditions beyond 46.8 h.

Considering the LCOH, the result of 8.1 $/$kg_{H2}$ in scenario 1, can be considered acceptable compared with the actual prices estimated in 6 $/$kg_{H2}$ (IRENA, 2021), nonetheless the SOEC mode is dedicated only to cover the minimal demand to supply the auxiliary during the longest interruption period recorded.

While, due to the higher SOEC utilization factor and annual hydrogen production volume in the second scenario, it is observed a result of 1.95 $/$kg_{H2}$. The value is in line with the price expectations for large quantities of $GH_2$ in the region, forecasted between 1 $/$kg_{H2}$ and 3 $/$kg_{H2}$ (IEA, 2019b) in order to be economically comparable with diesel and natural gas. On the other hand, the configuration requires substantial infrastructure investment for the hydrogen pipeline network (more than 12 M$), which could be a challenge in terms of project financing and deployment. However, such system architecture will guarantee a stronger system resiliency during extreme conditions (environmental conditions or maintenance/failure periods), from being able to supply 5 OWTs with the centralized diesel backup generator to being able to supply the whole wind farm with a decentralized energy storage approach and the possibility to exchange hydrogen within the internal distribution network to cover the neighbouring demand. Furthermore, since the LCOH is aligned the forecasted price in the areas, this means that not only it could be possible to provide a better backup supply by implementing the rSOC system, but also the hydrogen production could generate a new source of income for the wind farm power plant operator.

## 5. Conclusions

This work presented a new concept of hydrogen coupled with offshore wind turbines, also analysing the water desalination. It was investigated the possibility to use the rSOC technology as an onsite storage system to cover the auxiliaries demand during power shortage. Other than proposing a concept system architecture, its operation viability was simulated via a dynamic model of the integrated system. To do so, each component has been assessed and characterized. Additionally, considering the constraint represented by the space availability in the offshore context, it was analysed the system volumetric footprint.

Different control strategies have been implemented to assess the rSOC system, the first solely dedicated to the auxiliaries, while the second focused on maximizing the rSOC capacity factor and the subsequent hydrogen production. The results have shown the compatibility of the supply of the auxiliary systems of a 2.3 MW wind turbine with a 120/21 kWe rSOC system in electrolysis/fuel cell mode respectively, with a minimal impact on the annual energy production of the wind turbine. Moreover, considering the rSOC modularity, this process could be easily scalable for larger turbines. Moving to larger size could be fruitful from an economic point of view in terms of economy of scale.

With an export-based strategy, up to 15 tons of hydrogen could be produced exceeding the auxiliary demand. In this case, which represent the most demanding between the two strategies, only a 9.82% reduction in the wind turbine annual energy production is recorded. Economically this is translated in a LCOS of 401 $/MWh, comparable with competitive storage technologies, and in a LCOH of 1.95 $/$kg_{H2}$ which is in aligned with target hydrogen prices in the region.

The thermal availability from the rSOC will largely cover to the desalination thermal needs, representing a promising solution for small-scale onsite desalination systems in offshore environments. This latter consideration can also path the way to a freshwater export stream too, which combined with the hydrogen production can represent a solution to be reckoned with especially in arid zones.

Finally, a total encumbrance in the order to 22.3 $m^3$ has been evaluated for the whole system, which represent less than 2% of the turbine tower volume, as mere figure of merit.

In conclusion, the system thermal match between its components, the moderate energy volume demanded, and the reliability assured during ordinary and extraordinary OWT functioning was simulated and discussed. Additionally, the hydrogen produced by the local rSOC systems, could be a valuable and viable solution to provide storage services in offshore wind turbines or wind farms as well as a commodity to be exported and sold at a competitive price.

## CRediT authorship contribution statement

**Mario Lamagna:** Conceptualization, Methodology, Formal analysis, Investigation, Resources, Writing – original draft. **Andrea Monforti Ferrario:** Conceptualization, Software, Formal analysis, Investigation, Writing – original draft. **Davide Astiaso Garcia:** Validation, Investigation, Writing – review & editing, Supervision. **Stephen Mcphail:** Validation, Investigation, Writing – review & editing, Supervision. **Gabriele Comodi:** Validation, Investigation, Writing – review & editing, Supervision.

## Declaration of competing interest

The authors declare that they have no known competing financial interests or personal relationships that could have appeared to influence the work reported in this paper.

## Data availability

The authors do not have permission to share data.

## Acknowledgment

Authors would like to thank Vattenfall for the access to the SCADA data for Lillgrund Offshore Wind farm used for this study

## References

Ali Sha, K., et al., 2021. A synthesis of feasible control methods for floating offshore wind turbine system dynamics. Renew. Sustain. Energy Rev. 151, 111525.

Altaee, A., Mabrouk, A., Bourouni, K., Palenzuela, P., 2014. Forward osmosis pretreatment of seawater to thermal desalination: High temperature FO-MSF/MED hybrid system. Desalination 339, 18–25.

Altaee, A., Zaragoza, G., 2014. A conceptual design of low fouling and high recovery FO–MSF desalination plant. Desalination 343, 2–7.

Assiry, A.M., Gaily, M.H., Alsamee, M., Sarifudin, A., 2010. Electrical conductivity of seawater during ohmic heating. Desalination 260, 9–17.

Baldinelli, A., Barelli, L., Bidini, G., Cinti, G., Di Michele, A., Mondi, F., 2020. How to power the energy–water Nexus: Coupling desalination and hydrogen energy storage in mini-grids with reversible solid oxide cells. Processes 8, 1494.

Baptista, P., Costa, R., Ganilha, S., Armi, B., 2021. Assessment of offloading pathways for wind-powered offshore hydrogen production: Energy and economic analysis. Alied Energy 286, 116553.

Barbarelli, S., Nastasi, B., 2021. Tides and tidal currents—Guidelines for site and energy resource assessment. Energies 14 (19), 6123.

Bauer kompressoren, 2021. Mariner 200 compressor technical data. available at https://www.bauer-kompressoren.de/en/products/breathing-air-sports/profi-line-ii-140-320-lmin/mariner-200-200-lmin/. (Last opened 15 February 2021).

Beyrami, j., Chitsaz, A., Parham, K., Arild, Ø., 2019. Optimum performance of a single effect desalination unit integrated with a SOFC system by multi-objective thermo-economic optimization based on genetic algorithm. Energy 186, 115811.

Bodewes, F.J., 2017. Generating auxiliary power for a wind turbine. United States Patent.

Buffo, G., Ferrero, D., Santarelli, M., Lanzini, A., 2020. Energy and environmental analysis of a flexible power-to-X plant based on reversible solid oxide cells (rSOCs) for an urban district. J. Energy Storage 29, 101314.

Campione, A., Cipollina, A., Calise, F., Tamburini, A., Galluzzo, M., Micale, G., 2020. Coupling electrodialysis desalination with photovoltaic and wind energy systems for energy storage: Dynamic simulations and control strategy. Energy Convers. Manag. 216, 112940.

Cau, G., Cocco, D., Petrollese, M., Knudsen Kær, S., Milan, C., 2014. Energy management strategy based on short-term generation scheduling for a renewable microgrid using a hydrogen storage system. Energy Convers. Manag. 87, 820–831.

Chen, L., Wang, H., Liu, B., Wang, Y., Ding, Y., Pan, H., 2021. Battery state-of-health estimation based on a metabolic extreme learning machine combining degradation state model and error compensation. Energy 215, 119078.

Chitgar, N., Moghimi, M., 2020. Design and evaluation of a novel multi-generation system based on SOFC-GT for electricity, fresh water and hydrogen production. Energy 197, 117162.

Cioccolanti, L., Savoretti, A., Renzi, M., Caresana, F., Comodi, G., 2015. Design and test of a single effect thermal desalination plant using waste heat from m-CHP units. Appl. Therm. Eng. 82, 18–29.

Cioccolanti, L., Savoretti, A., Renzi, M., Caresana, F., Comodi, G., 2016. Comparison of different operation modes of a single effect thermal desalination plant using waste heat from m-CHP units. Appl. Therm. Eng. 100, 646–657.

Crivellari, A., Cozzani, V., 2020. Offshore renewable energy exploitation strategies in remote areas by power-to-gas and power-to-liquid conversion. Int. J. Hydrogen Energy 45, 2936–2953.

Dedecca, J.G., Hakvoort, R.A., Herder, P.M., 2017. Transmission expansion simulation for the European Northern Seas offshore grid. Energy 125, 805–824.

Dinh, V.N., Leahy, P., McKeogh, E., Murphy, J., Cummins, V., 2020. Development of a viability assessment model for hydrogen production from dedicated offshore wind farms. Int. J. Hydrogen Energy.

d'Amore Domenech, R., Santiago, Ó., Leo, T.J., 2020. Multicriteria analysis of seawater electrolysis technologies for green hydrogen production at sea. Renew. Sustain. Energy Rev. 113, 110166.

Elsaid, K., Kamil, M., Sayed, E.T., Abdelkareem, M.A., Wilberforce, T., Olabi, A., 2020. Environmental impact of desalination technologies: A review. Sci. Total Environ. 748, 141528.

Fan, L., Tu, Z., Chan, S.H., 2021. Recent development of hydrogen and fuel cell technologies: A review. Energy Rep. 7, 8421–8446.

Farhat, M., Yusuf, B., Tareq, A.A., 2021. Design and thermodynamic assessment of a solar powered energy–food–water nexus driven multigeneration system. Energy Rep. 7, 3033–3049.

Feroldi, D., Degliuomini, L.N., Basualdo, M., 2013. Energy management of a hybrid system based on wind-solar power sources and bioethanol. Chem. Eng. Res. Des. 91, 1440–1455.

Gallardo, F.I., Monforti Ferrario, A., Lamagna, M., Bocci, E., Astiaso Garcia, D., Baeza-Jeria, T.E., 2020. A techno-economic analysis of solar hydrogen production by electrolysis in the north of Chile and the case of exportation from Atacama Desert to Japan. Int. J. Hydrogen Energy 46, 13709–13728.

García-Rodríguez, L., 2003. Renewable energy alications in desalination: State of the art. Sol. Energy 75, 381–393.

Ghaffour, N., Missimer, T.M., Amy, G.L., 2013. Technical review and evaluation of the economics of water desalination: Current and future challenges for better water suly sustainability. Desalination 309, 197–207.

Göçmen, T., Giebel, G., 2016. Estimation of turbulence intensity using rotor effective wind speed in Lillgrund and Horns Rev-I offshore wind farms. Renew. Energy 99, 524–532.

Groppi, D., et al., 2021. A review on energy storage and demand side management solutions in smart energy islands. Renew. Sustain. Energy Rev. 135, 110183.

Guler, E., Ozakdag, D., Arda, M., et al., 2010. Effect of temperature on seawater desalination-water quality analyses for desalinated seawater for its use as drinking and irrigation water. Environ. Geochem. Health 32, 335–339.

GWEC, 2021. Global offshore wind report 2020. available at https://gwec.net/global-offshore-wind-report-2020/. (Last opened 3 March 2021).

Hauch, A., Ploner, A., Pylypko, S., Cubizolles, G., Mougin, J., 2021. Test and characterization of reversible solid oxide cells and stacks for innovative renewable energy storage. Fuel Cells 21 (5), 413–487.

Heydari, A., et al., 2020. Short-term electricity price and load forecasting in isolated power grids based on composite neural network and gravitational search optimization algorithm. Alied Energy 277, 115503.

Hou, P., Enevoldsen, P., Eichman, J., Hu, W., Jacobson, M.Z., Chen, Z., 2017. Optimizing investments in coupled offshore wind -electrolytic hydrogen storage systems in Denmark. Power Source 359, 186–197.

Hydrogen Council, 2021. Hydrogen insights 2021: A perspective on hydrogen investment, deployment and cost competitiveness'. available at https://hydrogencouncil.com/wp-content/uploads/2021/02/Hydrogen-Insights-2021.pdf. (Last opened 3 March 2021).

IEA, 2019a. Offshore Wind Outlook 2019. IEA, Paris, availabe at https://www.iea.org/reports/offshore-wind-outlook-2019. (Last opened 10 March).

IEA, 2019b. The Future of Hydrogen. IEA, Paris, https://www.iea.org/reports/the-future-of-hydrogen. (Last opened 03 August 2022).

IEA, 2020. Renewables 2020. IEA, Paris, available at https://www.iea.org/reports/renewables-2020. (Accessed 3 March 2021).

Ikäheimo, Jussi, Kiviluoma, Juha, Weiss, Robert, Holttinen, Hannele, 2018. ower-to-ammonia in future North European 100% renewable power and heat system. Int. J. Hydrogen Energy 43.

IRENA, 2021. Making the Breakthrough: Green Hydrogen Policies and Technology Costs. International Renewable Energy Agency, Abu Dhabi.

Jacobsson, S., Karltorp, K., 2013. Mechanisms blocking the dynamics of the European offshore wind energy industry – challenges for policy intervention. Energy Policy 63, 1182–1195.

Jesson, J., Larsen, P.E., Larsson, A., 2008. Technical Description Lillgrund Wind Power Plant. Tech. Rep. 2.1 Lillgrund Pilot Project, Vattenfall Vindkraft AB.

Kakoulaki, G., Kougias, I., Taylor, N., Dolci, F., Moya, J., Jäger-Waldau, A., 2021. Green hydrogen in Europe – A regional assessment: Substituting existing production with electrolysis powered by renewables. Energy Convers. Manage. 228, 113649.
Kim, J., Hong, S., 2018. Optimizing seawater reverse osmosis with internally staged design to improve product water quality and energy efficiency. J. Membr. Sci. 76–85.
Lamagna, M., Nastasi, B., Groi, D., Rozain, C., Manfren, M., Astiaso Garcia, D., 2021. Techno-economic assessment of reversible solid oxide cell integration to renewable energy systems at building and district scale. Energy Convers. Manage. 235.
Lazard, 2014. Lazard's levelized cost of energy analysis, version 8.0.
Lazard, 2018. Lazard's levelized cost of storage analysis, version 4.0.
Liponi, A., Wieland, C., Baccioli, A., 2020. Multi-effect distillation plants for small-scale seawater desalination: Thermodynamic and economic improvement. Energy Convers. Manage. 205, 112337.
Ma, S., Jiang, M., Tao, P., Song, C., Wu, J., Wang, J., Deng, T., Shang, W., 2018. Temperature effect and thermal impact in lithium-ion batteries: A review. Progress Nat. Sci.: Mater. Int. 28 (6), 653–666, 2018.
Majidi Nezhad, M., Neshat, M., Heydari, A., Razmjoo, A., Piras, G., Astiaso Garcia, D., 2021. A new methodology for offshore wind speed assessment integrating sentinel-1, ERA-interim and in-Situ measurement. Renew. Energy 172, 1301–1313.
Manfren, M., Nastasi, B., Tronchin, L., Groi, D., Astiaso Garcia, D., 2021. Techno-economic analysis and energy modelling as a key enabler for smart energy services and technologies in buildings. Renew. Sustain. Energy Rev. 150, 111490.
Mauler, L., Duffner, F., Zeier, W.G., Leker, J., 2021. Battery cost forecasting: A review of methods and results with an outlook to 2050. Energy Environ. Sci. 14, 4712–4739.
Meier, K., 2014. Hydrogen production with sea water electrolysis using norwegian offshore wind energy potentials: Techno-economic assessment for an offshore-based hydrogen production aroach with state-of-the-art technology. Int. J. Energy Environ. Eng. 5, 1–12.
Merkay, C., 2018. Tidal Park Within Offshore Wind Parks, an Analysis for the Potential Use of Tidal Kites Within the Aberdeen Offshore Wind Farm (M.Sc. Thesis). KTH Env. Eng. Dept..
Mogensen, M.B., Chen, M., Frandsen, H.L., Graves, C., Hansen, J.B., Hansen, K.V., et al., 2019. Reversible solid-oxide cells for clean and sustainable energy. Clean Energy 3, 175–201.
Monforti Ferrario, A., Vivas, F.J., Segura Manzano, F., Andujar, J.M., Bocci, E., Martirano, L., 2020. Hydrogen vs. battery in the long-term operation. A comparative between energy management strategies for hybrid renewable microgrids. Electronics 9, 1–27.
Nabiyan, M.S., Khoshnoudian, F., Moaveni, B., Ebrahimian, H., 2021. Mechanics-based model updating for identification and virtual sensing of an offshore wind turbine using sparse measurements. Struct. Control Health Monit. 28, e2647.
Nastasi, B., 2015. Renewable hydrogen potential for low-carbon retrofit of the building stocks. Energy Procedia 82, 944–949.
Nastasi, B., 2019. Hydrogen policy, market and R & D project. In: Calise, F., D'Accadia, M.D., Santerelli, M., Lanzini, A., Ferrero, D. (Eds.), Solar Hydrogen Production. Elsevier, Cambridge, MA, USA.
Nechache, A., Hody, S., 2019. Test and evaluation of an hybrid storage solution for buildings, based on a reversible high-temperature electrolyzer. ECS Trans. 91, 2485–2494.
Peters, R., Frank, M., Tiedemann, W., Hoven, I., Deja, R., Kruse, N., et al., 2021. Long-term experience with a 5/15kW-Class reversible solid oxide cell system. J. Electrochem. Soc. 168, 014508.
Peterson, D., 2020. Reversible fuel cell targets. DOE hydrogen and fuel cells program record.
Pourrahmani, H., Gay, M., Van herle, J., 2021. Electric vehicle charging station using fuel cell technology: Two different scenarios and thermodynamic analysis. Energy Rep. 7, 6955–6972.
Reichholf, F., Koberg, R., Schauperl, M., D., Hauth., 2020. Reversible SOC system development and testing: Status at AVL and outlook. In: 14th European SOFC & SOE Forum 2020. Lucerne Switzerland.
Ren, Z., et al., 2021. Offshore wind turbine operations and maintenances: A state of the art review. Renew. Sustain. Energy Rev. 144, 110886.
Reuß, M., Grube, T., Robinius, M., Preuster, P., Wasserscheid, P., Stolten, D., 2017. Seasonal storage and alternative carriers: A flexible hydrogen suly chain model. Appl. Energy 200, 290–302.
Rezk, H., 2019. Fuel cell as an effective energy storage in reverse osmosis desalination plant powered by photovoltaic system. Energy 175, 423–433.
Rezk, H., Nassef, A.M., Abdelkareem, M.A., Alami, A.H., Fathy, A., 2021. Comparison among various energy management strategies for reducing hydrogen consumption in a hybrid fuel cell/supercapacitor/battery system. Int. J. Hydrogen Energy 46.
Rispoli, N., Vitale, F., Califano, F., Califano, M., Polverino, P., Rosen, M.A., et al., 2020. Constrained optimal design of a reversible solid oxide cell-based multiple load renewable microgrid. J. Energy Storage 31, 101570.
Shengnan, X., Qingzheng, G., Weitao, Z., Lianying, W., 2022. Optimal scheduling of the combined power and desalination system. Energy Reports 8, 661–669.
Shepherd, A., Roberts, S., Sünnenberg, G., Lovett, A., Hastings, A.F.S., 2021. Scotland's onshore wind energy generation, impact on natural capital & satisfying no-nuclear energy policy. Energy Rep. 7, 7106–7117.
Shezan, S.K.A., 2021. Feasibility analysis of an islanded hybrid wind-diesel-battery microgrid with voltage and power response for offshore islands. J. Cleaner Prod. 288.
Siemens, 2009. Wind turbine SWT-2.3-93 technical datasheet.
Signorato, F., Morciano, M., Bergamasco, L., Fasano, M., Asinari, P., 2020. Exergy analysis of solar desalination systems based on passive multi-effect membrane distillation. Energy Rep. 6, 445–454.
Solid Power, 2021. Bluegen micro cogeneration data sheet. available at https://www.solidpower.com/it/bluegen/per-gli-installatori/. (Last opened 12 February 2021).
Statista, 2022. Average monthly electricity wholesale price in Sweden from january 2019 to may 2022 (in euros per megawatt-hour). https://www.statista.com/statistics/1271491/sweden-monthly-wholesale-electricity-price/. (Last opened 03 August 2022).
Suman, G.K., Guerrero, J.M., Prakash Roy, O., 2021. Optimisation of solar/wind/bio-generator/diesel/battery based microgrids for rural areas: A PSO-GWO aroach. Sustainable Cities Soc. 67.
Timothy, D.H., Siyuan, D., Rachel, L., Solomon, B., 2021. Long term energy storage with reversible solid oxide cells for microgrid alications. Energy Rep. 7 (Sulement 2).
Ullvius, N.C., Rokni, M., 2019. A study on a polygeneration plant based on solar power and solid oxide cells. Int. J. Hydrogen Energy 44, 19206.
Vattenfall, 2022. For what and to whom will I pay?. https://www.vattenfall.se/english/about-your-invoice/. (Last opened 03 August 2022).
Venkataraman, V., Pérez-Fortes, M., Wang, L., Hajimolana, Y.S., Boigues-Muñoz, C., Agostini, A., et al., 2019. Reversible solid oxide systems for energy and chemical alications – review & perspectives. J. Energy Storage 24, 100782.
Wang, Y., Banerjee, A., Wehrle, L., Shi, Y., Brandon, N., Deutschmann, O., 2019. Performance analysis of a reversible solid oxide cell system based on multi-scale hierarchical solid oxide cell modelling. Energy Convers. Manag. 196, 484–496.
Wang, X., Christ, A., Regenauer-Lieb, K., Hooman, K., Chua, H.T., 2011. Low grade heat driven multi-effect distillation technology. Int. J. Heat Mass Transf. 54, 5497–5503.
Wang, Y., Leung, D.Y.C., Xuan, J., Wang, H., 2017. A review on unitized regenerative fuel cell technologies, Part B: Unitized regenerative alkaline fuel cell, solid oxide fuel cell, and microfluidic fuel cell. Renew. Sustain. Energy Rev. 75, 775–795.
Wang, Y., Li, W., Ma, L., Li, W., Liu, X., 2020. Degradation of solid oxide electrolysis cells: Phenomena, mechanisms, and emerging mitigation strategies—A review. J. Mater. Sci. Technol. 55, 35–55.
Wind europe, 2021. Offshore wind in Europe key trends and statistics 2019. available at https://windeurope.org/about-wind/statistics/offshore/european-offshore-wind-industry-key-trends-statistics-2019/#:~:text=Check%20the%20presentation-,Overview,wind%20turbines%20across%2012%20countries. (Accessed 3 March 2021).
Wu, Yunna, Liu, Fangtong, Wu, Junhao, He, Jiaming, Xu, Minjia, Zhou, Jianli, 2022. Barrier identification and analysis framework to the development of offshore wind-to-hydrogen projects. Energy 239 (Part B).
Wu, X., et al., 2019. Foundations of offshore wind turbines: A review. Renew. Sustain. Energy Rev. 104, 379–393.
Xu, X., Hu, W., Cao, D., Huang, Q., Liu, Q., Chen, C., Lund, H., Chen, Z., 2020. Economic feasibility of a wind-battery system in the electricity market with the fluctuation penalty. J. Cleaner Prod. 271.
Xueqing, Z., Rui, Q., Meng, Y., Qi, L., Yamin, Y., Yongtu, L., Haoran, Z., 2021. Sustainable offshore oil and gas fields development: Techno-economic feasibility analysis of wind–hydrogen–natural gas nexus. Energy Rep. 7, 4470–4482.
Yanan, Z., Mingliang, L., Rui, L., Zhichun, L., Wei, L., 2021. Advanced adsorption-based osmotic heat engines with heat recovery for low grade heat recovery. Energy Rep. 7, 5977–5987.
Yue, M., Lambert, H., Pahon, E., Roche, R., Jemei, S., Hissel, D., 2021. Hydrogen energy systems: A critical review of technologies, alications, trends and challenges. Renew. Sustain. Energy Rev. 146, 111180.
Zahedi, Rahim, Ahmadi, bolfazl, Sadeh, Mohammad, 2021. Investigation of the load management and environmental impact of the hybrid cogeneration of the wind power plant and fuel cell. Energy Report. 7, 2930–2939.
Zhao, F., et al., 2022. Control interaction modeling and analysis of grid-forming battery energy storage system for offshore wind power plant. IEEE Trans. Power Syst. 37 (1), 497–507.